

Disorders of the Nervous System

Deletion of *Sod1* in Motor Neurons Exacerbates Age-Related Changes in Axons and Neuromuscular Junctions in Mice

N. Pollock,¹  P. C. Macpherson,² C. A. Staunton,¹ K. Hemmings,¹ C. S. Davis,² E. D. Owen,¹ A. Vasilaki,¹ H. Van Remmen,³ A. Richardson,⁴ A. McArdle,¹ S. V. Brooks,^{2,*} and M. J. Jackson^{1,*}

<https://doi.org/10.1523/ENEURO.0086-22.2023>

¹Department of Musculoskeletal and Ageing Science, Institute of Life Course and Medical Sciences, University of Liverpool, and MRC-Versus Arthritis Centre for Integrated Research into Musculoskeletal Ageing (CIMA), Liverpool, L7 8TX, UK, ²Molecular and Integrative Physiology, University of Michigan, Ann Arbor, 48109 MI, ³Oklahoma Medical Research Foundation (OMRF), Oklahoma City, 73104, OK, and ⁴University of Oklahoma Health Science Center (OUHSC), Oklahoma City, 73104, OK

Abstract

Whole-body knock-out of Cu,Zn superoxide dismutase (Sod1KO) results in accelerated, age-related loss of muscle mass and function associated with neuromuscular junction (NMJ) breakdown similar to sarcopenia. In order to determine whether altered redox in motor neurons underlies this phenotype, an inducible neuron-specific deletion of Sod1 (i-mnSod1KO) was compared with wild-type (WT) mice of different ages (adult, mid-age, and old) and whole-body Sod1KO mice. Nerve oxidative damage, motor neuron numbers and structural changes to neurons and NMJ were examined. Tamoxifen-induced deletion of neuronal Sod1 from two months of age. No specific effect of a lack of neuronal Sod1 was seen on markers of nerve oxidation (electron paramagnetic resonance of an *in vivo* spin probe, protein carbonyl, or protein 3-nitrotyrosine contents). i-mnSod1KO mice showed increased denervated NMJ, reduced numbers of large axons and increased number of small axons compared with old WT mice. A large proportion of the innervated NMJs in old i-mnSod1KO mice displayed a simpler structure than that seen in adult or old WT mice. Thus, previous work showed that neuronal deletion of Sod1 induced exaggerated loss of muscle in old mice, and we report that this deletion leads to a specific nerve phenotype including reduced axonal area, increased proportion of denervated NMJ, and reduced acetyl choline receptor complexity. Other changes in nerve and NMJ structure seen in the old i-mnSod1KO mice reflect aging of the mice.

Key words: axon; motor unit; oxidative stress; skeletal muscle

Significance Statement

Sarcopenia is the age-related loss of muscle mass and function. It is a significant contributor to frailty and to increased falls in the elderly. While multifactorial, changes in redox status have been shown to have significant influence over neuromuscular aging, recent work suggests that changes in motor neurons may be the driving factor in muscle atrophy. The current study confirmed that a specific lack of Sod1 in the motor neuron causes significant alteration in axonal architecture and the neuromuscular junctions (NMJs), which can drive reduced muscle mass and function. Pinpointing early changes in motor neurons may provide therapeutic targets critical for maintaining muscle in the elderly.

Received February 24, 2022; accepted February 5, 2023; First published February 21, 2023.

The authors declare no competing financial interests.

Author contributions: N.P., P.C.M., C.A.S., K.H., C.S.D., E.D.O., and A.V. performed research; N.P., P.C.M., C.A.S., A.V., H.V.R., A.R., A.M., S.V.B., and M.J.J. analyzed data; N.P., P.C.M., A.M., S.V.B., and M.J.J. wrote the paper; H.V.R., A.R., A.M., S.V.B., and M.J.J. designed research.

Introduction

The cross-sectional area (CSA) of skeletal muscle in humans is reduced by 25–30% and muscle strength by 30–40% by age 70 (Porter et al., 1995). The reduction in muscle mass and function with age is because of a decrease in the number of muscle fibers and atrophy and weakening of those remaining (Lexell et al., 1986, 1988; Brooks and Faulkner, 1988). The loss of muscle that occurs with aging occurs in parallel with loss of motor units in both humans and rodents (Campbell et al., 1973; Sheth et al., 2018) and is associated with a 25–50% reduction in the number of motor neurons (Tomlinson and Irving, 1977; Rowan et al., 2012; Piekarczyk et al., 2020). This appears to be because of selective loss of large fast α -motor neurons leading to an apparent increase in the proportion of Type I (slow twitch) or Type IIa muscle fibers that is particularly apparent in humans (Narici and Maffulli, 2010; Sonjak et al., 2019). Loss of innervation of individual fibers occurs in muscles with aging and we previously reported that ~15% of individual muscle fibers in old mice are completely denervated and ~80% of neuromuscular junctions (NMJs) showed some disruption (Vasilaki et al., 2016).

In order to examine the potential role of oxidative stress and redox changes in aging, we previously examined the effect of a lack of superoxide dismutase1 (Sod1) in whole-body knock-out mice (Sod1KO) and demonstrated an accelerated loss of muscle mass and function that is associated with a breakdown of NMJs (Jang et al., 2010; Larkin et al., 2011). Adult mice lacking Sod1 exhibit many features observed in old wild-type (WT) mice (>24 months) including loss of muscle force, altered mitochondrial function and an accumulation of structural alterations at NMJs. Subsequent studies examined the effects of specific deletion of Sod1 in muscle (mSod1KO; Sakellariou et al., 2018) or motor neurons (nSod1KO; Sataranatarajan et al., 2015), but both models exhibited only a mild muscle phenotype, while expression of human SOD1 specifically in neurons of Sod1KO model was found to “rescue” the phenotype such that no premature loss of muscle mass nor alterations in NMJ structure were observed (Sakellariou et al., 2014).

To address the possibility that embryonic neuronal Sod1 knock-down in the nSod1KO mice induced a compensatory effect, we have recently created an inducible motor neuron Sod1 KO (i-mnSod1KO) mouse model (Bhaskaran et al., 2020) to examine whether loss of Sod1 in motor neurons in adult-life affected age associated

muscle wasting and weakness. These mice were found to have an age-related, accelerated loss of muscle mass which preceded that seen in old WT mice by six to eight months (Bhaskaran et al., 2020).

In the current study, we examine the effects of age and lack of Sod1 specifically in neurons on motor neuron number and explore the changes in nerve oxidation status as well as structural changes in axons and NMJs. Our aim was to define whether a neuron-specific lack of CuZnSOD would be sufficient to compromise neuronal oxidation, induce disruptions of neuronal and NMJ structure, and increase denervation.

Materials and Methods

Mice

The neuron specific inducible Sod1 knock-out mice (i-mnSod1KO) used in this study were tamoxifen-induced KOs (10 mg/ml tamoxifen administered at two and four months) generated as previously described at the Oklahoma Medical Research Foundation (OMRF; Bhaskaran et al., 2020). In order to understand the specific role of neuronal Sod1 in the premature loss of neuronal and muscle structure and mass, the i-mnSod1KO mice were compared with age-matched WT mice in three distinct groups: six to nine months (adult), 16–18 months (mid-age), and 24–29 months (old). The i-mnSod1KO mice were also compared with whole-body knock-out (Sod1KO) mice. Whole-body Sod1KO mice were bred at OMRF as previously described (Sakellariou et al., 2014). Mice were maintained under specific pathogen-free (SPF) conditions and shipped to the University of Liverpool or the University of Michigan, where they were maintained until required. Whole-body Sod1KO mice were also crossed with Thy1-CFP mice (The Jackson Laboratory) at the University of Liverpool to produce mice (Sod1KO-Thy1-CFP) expressing CFP in neurons to allow ready visualization of the nerve without the need for antibody staining. These mice had the phenotypic changes observed in founder Sod1KO mice. The SlickH Cre mouse used to generate i-mnSod1KO mice were originally developed as a model to delete genes in motor neurons, while also simultaneously labeling the neurons with YFP and hence all expressed YFP in motor neurons (Bhaskaran et al., 2020). Male and female mice were used throughout this study.

All mice were fed *ad libitum* on a standard laboratory diet, subjected to a 12/12 h light/dark cycle and maintained under SPF conditions. All experiments were performed in accordance with UK Home Office guidelines under the UK Animals (Scientific Procedures) Act 1986 and received ethical approval from the University of Liverpool Animal Welfare Ethical Review Body (AWERB).

Functional data

Extensor digitorum longus (EDL) force data were gathered *in situ* as previously described (Brooks and Faulkner, 1988). Briefly, with the mouse under terminal anesthesia the whole EDL muscle was isolated, the distal tendon was severed and secured to the lever arm of a servomotor and the muscle was activated by stimulation of the peroneal nerve.

This work was supported by the National Institute on Aging Grant AG051442, the Medical Research Council Grant MR/M012573/1, and the University of Liverpool.

Acknowledgments: We thank the Biomedical Services Unit, University of Liverpool for excellent animal care throughout the project.

*S.V.B. and M.J.J. are joint senior authors.

Correspondence should be addressed to M. J. Jackson at mjj@liverpool.ac.uk.
<https://doi.org/10.1523/ENEURO.0086-22.2023>

Copyright © 2023 Pollock et al.

This is an open-access article distributed under the terms of the Creative Commons Attribution 4.0 International license, which permits unrestricted use, distribution and reproduction in any medium provided that the original work is properly attributed.

Maximum isometric tetanic force (Po) was recorded and specific Po was calculated from cross-sectional area (CSA) of the EDL. Mice were subsequently killed by a schedule 1 procedure and sciatic nerves rapidly excised and used for biochemical analyses.

Oxidation markers

Electron paramagnetic resonance

In order to define the activity of specific reactive oxygen species (ROS) in muscle and nerve an *in vivo* electron paramagnetic resonance spin probe protocol using 1-hydroxy-3-carboxy-2,2,5,5-tetramethylpyrrolidine (CPH; Noxygen) was used as previously described (McDonagh et al., 2016). The CPH probe was made up in PBS containing sodium diethyldithio-carbamate trihydrate (DETC; 5 μM) and desferoxamine methane sulfonate salt (DF; 25 μM) fresh before each procedure. Groups of mice were anaesthetized via inhalation of isoflurane (2%) and maintained at an appropriate level in this manner via nose cone throughout this procedure. Mice received a tail vein bolus injection (80 μl , 9 mg/kg body weight) followed by tail vein infusion (0.225 $\mu\text{g}/\text{kg}$ body weight/min) of the probe for 2 h. The mice were killed by cervical dislocation and the sciatic nerve and gastrocnemius muscle were quickly excised, stored in Krebs buffer and frozen in liquid nitrogen. Samples were stored in liquid nitrogen in a vapor phase Dewar. In order to detect levels of the oxidized probe 3-carboxy-proxyl radical (CP), samples were placed into the finger Dewar of the Bruker e-scan benchtop EPR and scanned using the settings: microwave frequency 9.78 GHz, modulation frequency 86 kHz, modulation amplitude 6.15 G, gain 10^3 .

Western blot analysis. Following killing, sciatic nerve was quickly excised and snap frozen in liquid nitrogen. The frozen nerves were cryo-pulverized under liquid nitrogen and the resulting powder added to 40 μl RIPA buffer (Merck Millipore) $10\times$ diluted with distilled water with protease inhibitors (Roche, complete, mini, EDTA-free protease inhibitor cocktail). Samples were sonicated on ice, centrifuged at $12,000 \times g$ for 10 min at 4°C and the supernatant retained. Protein content was quantified by BCA assay. 20 μg of total protein per sample was separated by SDS-PAGE with 4% stacking and 12% resolving gels. Electrophoresis was conducted at 120 V for protein separation, followed by semi-dry transfer onto nitrocellulose membrane for 1.5 h at 300 mA (Bio-Rad Trans-Blot SD).

A Ponceau S (Sigma) stain was used to verify the effectiveness of protein transfer. The membrane was blocked using 5% fish skin gelatin (FSG) made up in Tris buffered saline with Tween blocking buffer (5% FSG TBS) for 1.5 h. The membranes were incubated with primary antibody against 3-nitrotyrosines (3-NTs; Abcam; 1:1000 dilution in 5% FSG TBS-T) overnight at 4°C . Duplicate gels were run to assess protein carbonyls using a kit which derivatizes proteins directly on the membrane following transblotting (Cell Biolabs). For this, proteins were transferred onto PVDF membrane, and derivatized as per manufacturer's instructions, and subsequently incubated with primary antibody against DNP (Cell Biolab; 1:1000 dilution 5% FSG TBS-T) overnight at 4°C . All membranes were then

washed with TBST, and incubated with appropriate secondary antibodies for 1 h (1:20,000 dilution in 5% FSG TBST with 0.01% SDS). Protein bands were visualized on a Licor Odyssey CLx imaging system.

Sciatic nerve cross-sections

Sciatic nerves were dissected (from point of bifurcation at the knee up to the spinal column), placed onto a needle (to prevent curling and maintain orientation) and submerged in 10% neutral buffered formalin (NBF) overnight. Nerves were transferred into a 30% sucrose solution for cryo-protection for 5 d before embedding in colored OCT (Shandon Cryochrome) using cryomolds and freezing in liquid nitrogen cooled isopentane. Transverse sections (7 μm) of the nerve were cut on a cryostat (Leica CM1850). Sections were thawed, blocked in 5% goat serum for 1 h and stained using myelin protein zero (MPZ; 1 in 50 in 5% goat serum in PBS containing 1% Triton X-100; EPR20383, Abcam) overnight. Following incubation with Alexa Fluor-594 nm secondary slides were mounted in hard-set mountant with Dapi (Vectorlabs) and visualized on Zeiss LSM800 confocal microscope using $40\times$ objective.

Image analysis was conducted using the free hand tool in ImageJ software (NIH). The axon and the outer edge of the stained myelin sheath of 100 axons were drawn around to provide area of the axon, area of the sheath and the distribution of axon sizes. G-ratios were calculated for each axon as the ratio of the inner axonal diameter to the total outer diameter including myelin sheath.

Retrograde motor neuron labeling

In separate experiments, mice were anesthetized with 3% isoflurane/oxygen and the nerve branches to medial and lateral heads of the left gastrocnemius were exposed and transected. On the contralateral side the sciatic nerve was transected at the level of the mid-thigh. Motor neurons were retrograde labeled by placing sterile Gelfoam saturated with 10% FluoroRuby (Invitrogen) over the respective nerve stumps, suturing the Gelfoam in place and closing the incision sites for recovery. Postoperative analgesia was achieved by treating mice with Carprofen (5 mg/kg) daily for 3 d. Following schedule 1 cull, the lumbar regions of spinal cords were obtained by extrusion with 5 ml of PBS 7 d after the onset of labeling. Spinal cords were fixed overnight in 10% formalin at 4°C , rinsed in PBS and processed for optical clearing according to previously published work (Ertürk et al., 2012; Žygelytė et al., 2016). Labeled motor neurons were imaged using an Olympus FV1000 confocal microscope with the z-step size set at 4.5 μm . Z-stacks were visualized using ImageJ and the total number of labeled motor neurons were quantified with the use of the cell counter plug-in function while scrolling through z-stacks.

NMJ analysis

NMJ analysis was conducted on EDL muscles with 20–60 NMJs per muscle analyzed. All mice utilized for these studies expressed a fluorescent protein in the nerves to allow ready visualization.

The EDL muscles were quickly excised following schedule 1 cull, pinned at roughly resting length onto sylgard plates (Femell) and fixed in 10% NBF. Whole EDL muscles were incubated with α -bungarotoxin conjugated Alexa Fluor-647 nm (1:1000; Invitrogen) in PBS (1% Triton X-100) for 30 min. Muscles were imaged via confocal microscopy (Nikon A1). The components of the NMJs were visualized using 488 nm laser to excite the YFP in the i-mnSod1KO, 405 nm to excite CFP in Sod1KO-CFP and the WT litter mates. Images were collected via 10 \times or 60 \times water immersion lens (Nikon). Z-stacking (1- to 2- μ m step) allowed for 3D evaluation of the NMJs.

Using NIS-elements software (Nikon) individual NMJs were identified and the ROI tool used to obtain the area of the muscle fiber that is occupied by individual NMJs. All NMJs were assessed and graded according to five separate measures of integrity and structure: (1) overlap of the presynaptic and postsynaptic regions (innervated, partial or denervated) and the (2) number of postsynaptic fragments (none, no fragmentation, <5, or >5 fragments), (3) the number of axonal sprouts and blebs, (4) the incidence of multi-innervated NMJs, and (5) the complexity of the NMJ. This classification ranged from “complex,” showing the typical structure seen in adult WT NMJ, to “basic,” in which the NMJ appeared as simple discs with little internal structure and resembled embryonic NMJs. One intermediate grade between complex and basic (“good”) was also used.

Experimental design and statistical analysis

For all experiments the number of mice used are indicated in the associated figure legend. All statistics were conducted using GraphPad Prism 8 software, unless stated otherwise results are presented as mean \pm SD.

For NMJ analysis, all NMJs present within a field of view were assigned an ID and counted/graded. Multiple 3D images per muscle were assessed and all measures were expressed as a percentage of the total number of NMJs in an image to correct for variation in the total number of NMJs seen in each image. For fragmentation, overlap and complexity two-way ANOVA with Tukey’s multiple comparisons was used, while for other measures one-way ANOVA with either Dunnett’s or Tukey’s multiple comparisons was used.

For Western blot analyses, it was only possible to load $n = 1$ onto each SDS gel for each group. In order to compare across gels the same muscle lysate was added to each and all results were normalized to this. The data were analyzed via one-way ANOVA. EPR data and force were also analyzed by one-way ANOVA. Significance values * $p < 0.05$, ** $p < 0.01$, *** $p < 0.001$, **** $p < 0.0001$.

Wherever possible multiple analyses were undertaken on the nerve and muscle from each mouse. This was not possible for mice that underwent perfusion of spin probe for EPR analysis, or used for retrograde labeling, where separate mice were examined.

Results

The i-mnSod1KO mice were previously reported to show an exaggerated age-associated loss of gastrocnemius muscle mass and function (Bhaskaran et al., 2020). This

was confirmed for the current cohort of old i-mnSod1KO mice where EDL force generation was reduced by $\sim 24\%$ compared with age-matched WT mice (data not shown).

Oxidation markers in nerve and muscle tissue

The concentration of the EPR adduct, CP in sciatic nerves of adult Sod1KO mice was significantly increased compared with adult WT mice (Fig. 1a), but WT and i-mnSod1KO mice showed no age associated changes in the amplitude of the EPR signal. Studies of the EPR signal in the TA muscle were also undertaken and these showed an increase in the old WT mice. Muscle of Sod1KO mice also showed a significantly higher EPR signal than WT controls (Extended Data Fig. 1-1). In addition, in accordance with previously published data (McDonagh et al., 2016), the sciatic nerve was also observed to have a much higher EPR signal compared with skeletal muscle (Fig. 1a; Extended Data Fig. 1-1).

Western blot analyses for protein carbonyls (Fig. 1b) revealed no statistically significant differences in sciatic nerves from any of the groups of KO or transgenic mice compared with WT mice either when the densitometry of the whole lane was assessed or when the four main bands were analyzed separately. Protein 3-nitrotyrosine (3-NT) levels were also examined (Fig. 1c). Few bands were detectable on the Western blottings of nerves for 3-NT with no evidence of any change that was specifically because of lack of Sod1 in 3NTs between the groups on raw densitometric analysis or following normalization to GAPDH content. In these latter analyses, the major band detected (~ 55 kDa) was also present in the negative control and likely to be because of nonspecific binding. Thus, there was no evidence for any specific increase in oxidation in nerves of the i-mnSod1KO mice.

Sciatic nerve morphology

Representative images of transverse sections through the sciatic nerve of each experimental group are shown in Figure 2a. Quantitative data for individual axonal area and the area of the myelin sheath around those axons was obtained. Axonal areas are shown in Figure 2b, there was no significant change in axonal area in old WT compared with adult WT mice. Axons from old i-mnSod1KO were significantly reduced in area in comparison with old WT mice. The distribution in axonal areas in each group is shown in Figure 2c and shows that there was a significant decrease of the larger axons ($>15 \mu\text{m}^2$) and increase in the proportion of small axons in the old i-mnSod1KO and Sod1KO mice.

The myelin areas for different sizes of axons are presented in Figure 2d. An increase in myelin area was seen for the larger axons in the old WT mice compared with adult mice and this was also seen in the old i-mnSod1KO mice, indicating an age-related change. The G-ratio is commonly used to assess the degree of myelination and is considered a marker of efficient signal conduction (Chomiak and Hu, 2009) and when G ratios were calculated from the above data no significant differences between groups were seen (Fig. 2e). In summary, these data

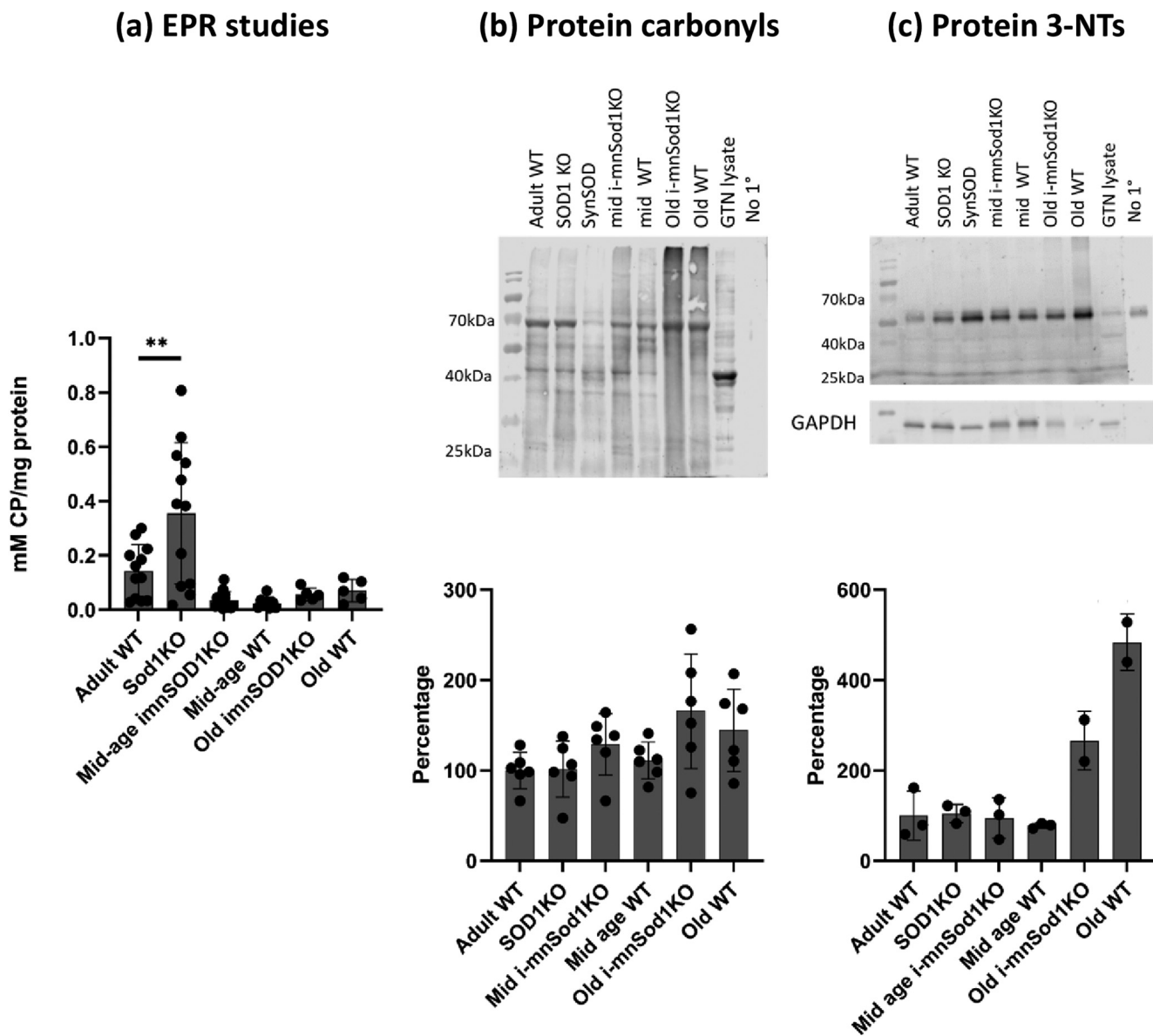


Figure 1. Markers of oxidation/oxidative damage in sciatic nerves of adult, mid-age and old WT, mid-age and old i-mnSod1KO and Sod1KO mice. Concentrations of CP, the EPR spin adduct in sciatic nerve ($n=6-14$; **a**). Representative Western blotting and quantification of protein carbonyl (**b**) and protein 3-NT (**c**) contents in sciatic nerve ($n=6$). Densitometry of the whole lane was undertaken and data are presented as mean \pm SD. Symbols represent significant differences compared with adult WT $**p < 0.01$, from one way ANOVA analysis with Dunnett comparison. Key: GTN-lysate = lysate of mouse gastrocnemius muscle used as a positive control sample; no 1° = lane in which no primary antibody added to determine nonspecific binding artefacts. In **c**, only two samples were analyzed from old i-mnSod1KO and old WT mice because of lack of available sample and statistical analysis of these lanes has not been undertaken. In the original Western blottings shown nerve samples from Sod1KO mice in which Sod1 was transgenically replaced in neuronal tissue (SynSOD mice, lane 4) were also examined but these data have been reported elsewhere and are not reported here. Extended Data Figure 1-1 shows EPR analysis of the concentration of CP in skeletal muscle from the experimental groups.

indicate that old i-mnSod1KO mice had a decreased number of large axons and increased number of small axons compared with age-matched WT mice.

Motor neuron quantification

Images illustrating the localization of the retrograde label to the lumbar spinal cord (Fig. 3A) and to the lateral ventral horn (Fig. 3B) after sciatic nerve transection demonstrate the suitability of this approach to specifically

label motor neurons. We evaluated changes in motor neuron numbers specifically innervating the gastrocnemius muscle (Fig. 3C) and more generally for motor neurons of all the muscles associated with the sciatic nerve (Fig. 3D). In both situations a significant decline in the number of motor neurons was found in old WT compared with adult WT mice. The declines in axon numbers were also seen in old i-mnSod1KO mice. The percentage of motor neuron loss with age was $\sim 30\%$ for both gastrocnemius specific

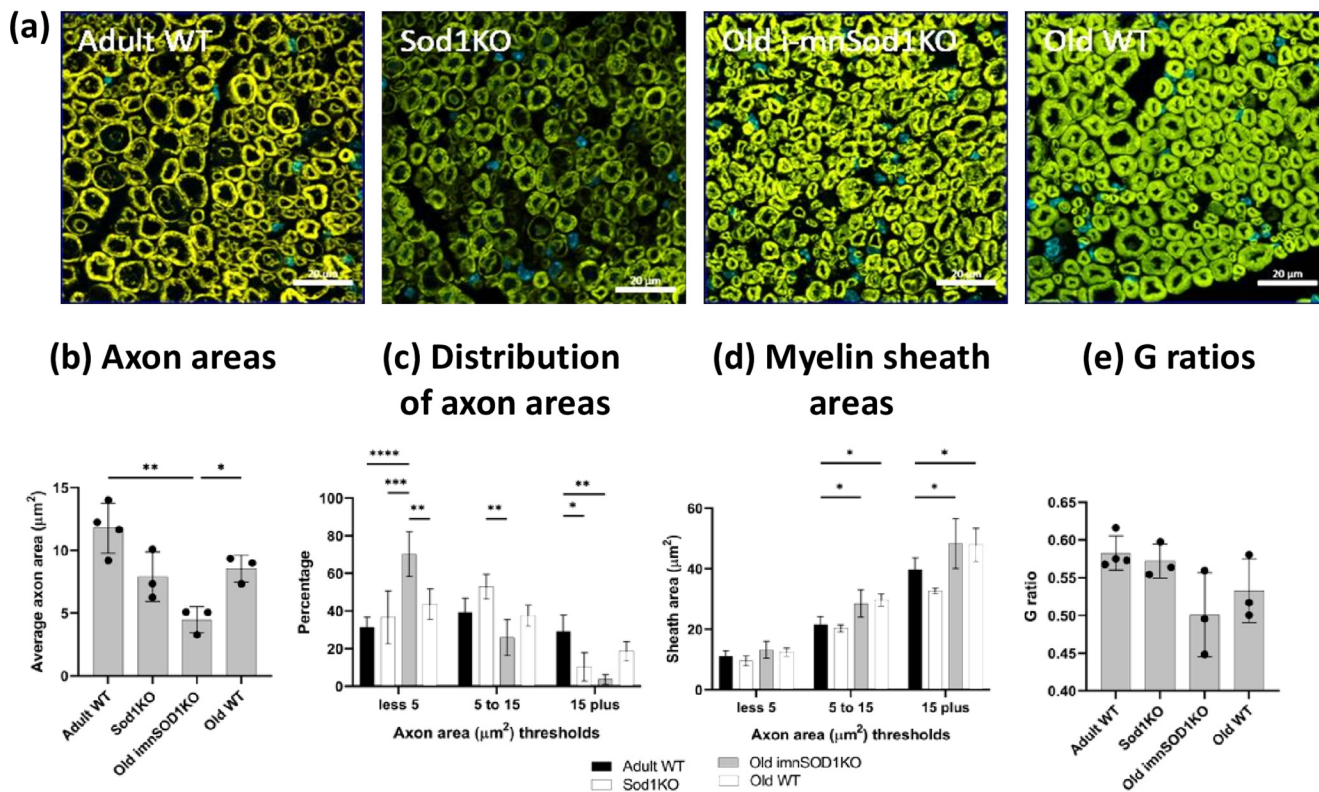


Figure 2. Morphology of sciatic nerves. Representative transverse cross-sections from adult and old WT mice, old i-mnSod1KO and Sod1KO mice are shown (a). Average axonal area (b), the distribution of axonal size (c), average myelin sheath area of axons categorized by axon size (d), and G-ratio (e) for adult, mid-age and old WT, mid-age and old i-mnSod1KO and Sod1KO mice. Scale bar = 20 μm . Data are presented as mean \pm SD. Symbols represent significant differences ($*p < 0.05$, $**p < 0.01$, $***p < 0.001$, $****p < 0.0001$) from two-way ANOVA analysis with Tukey's comparison ($n = 4$ nerves/group).

and whole sciatic nerve evaluations, but we found no additional loss of motor neurons attributable to the lack of Sod1.

Changes in NMJ structure

Images of NMJs from EDL muscles were captured via confocal microscopy to allow detailed examination of their structure. Figure 4a provides representative examples from z-stacked images of NMJ from adult, mid-age and old WT mice, Sod1KO mice and mid-age and old i-mnSod1KO mice. In these images the AchR clusters were stained with bungarotoxin and the nerve visualized via CFP or YFP expression. Axonal organization is clear and defined in adult WT but is highly disordered in both old WT and old i-mnSod1KO mice.

The average area of the muscle fiber occupied by individual NMJs showed no significant alteration either with advancing age or between any of the knock-out mouse models (data not shown). Overlap of presynaptic and postsynaptic regions was quantified and is shown in Figure 4b, i-iii. Fully innervated NMJ had complete overlap, partially innervated NMJ meant that some of the AchRs were visible without YFP overlay and in fully denervated only AchRs were visible. The values are expressed as a percentage of the total number of NMJs counted per muscle. NMJs in muscle from adult WT mice were

effectively fully innervated. NMJs from Sod1KO mice were found to be variable with roughly equivalent proportion innervated, partially innervated and denervated. At mid-age the WT and i-mnSod1KO mice had very similar profiles and showed some partially or fully denervated NMJs, but the changes were not significantly different to WT adult mice. There was a significant loss of fully innervated NMJs in both old WT ($p = 0.0071$) and old i-mnSod1KO ($p < 0.0001$), but this loss was significantly greater in the old i-mnSod1 mice with $< 15\%$ of NMJ remaining fully innervated [Fig. 4b(i)].

Fragmentation of the NMJ endplates was quantified [Fig. 4c(i-iii)] by counting the number of AchR clusters that were clearly separate and these were categorized as previously (Staunton et al., 2019). An intact endplate was recorded where no fragments were seen, this accounted for almost 70% of NMJs in adult WT mice [Fig. 4c(i)]. The mid-aged WT and mid-aged i-mnSod1KO mice were not significantly different to each other or to adult WT mice with respect to the number of intact endplates. There was a significant decline in intact endplates in both old WT ($p < 0.0001$) and old i-mnSod1KO mice compared with adult WT ($p < 0.0001$) and their own mid-age groups. This decline in intact endplates in both of the old groups was associated with a significant increase in the highly fragmented (more than five fragments) endplates observed in both

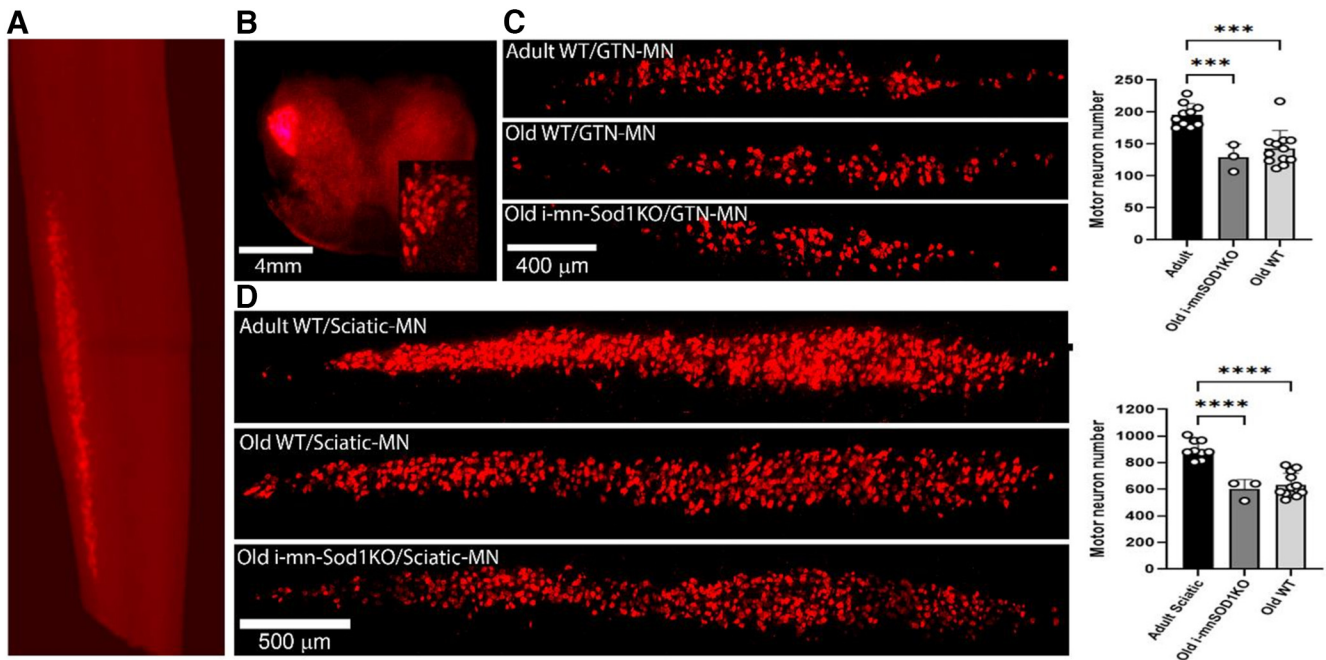


Figure 3. Quantification of motor neurons identified by retrograde labeling via transection of whole sciatic and the tibial nerve branches to the gastrocnemius. Representative images to show specific localization of the retrograde label to the lumbar spinal cord (**A**) and to the lateral ventral horn (**B**) after sciatic nerve transection (inset displays labeled individual motor neurons). Typical pattern of labeling of motor neurons in adult and old WT and old i-mnSOD1KO mice and quantification of numbers of labeled motor neurons following: transection of the nerve branches innervating the medial and lateral heads of the gastrocnemius (**C**), transection of the whole sciatic nerve (**D**). Data are presented as mean \pm SD; *** $p < 0.001$ from two-way ANOVA ($n = 3$ –12 animals per group).

groups [Fig. 4c(iii)]. There were no significant differences between the age-matched groups in any of the categories indicating there was no specific effect on AchR fragmentation that could be attributed to the lack of Sod1 rather than the age of the mice.

Sprouting of axons and the presence of blebs on the axons were assessed. Figure 5a(i) shows an example image illustrating multiple sprouting axons and Figure 5a(ii) shows the percentage of axons in which sprouting was evident. There was no evidence of sprouting in the adult WT groups but the percentage of sprouts increased significantly in the old WT and i-mnSod1KO groups of mice. An example image illustrating multiple axonal blebs is shown in Figure 5b(i) and the percentage of axons having blebs in each group is shown in Figure 5b(ii). A significant increase in the percentage of axons showing blebs was seen in the Sod1KO mice and in both mid-aged WT and i-mnSod1KO mice with no significant increase in the old groups.

Multiple innervation of single NMJs is also occasionally seen in samples from older mice and this was examined in the groups. Figure 5c(i) shows an example image illustrating multiple axonal innervation of a NMJ and Figure 5c(ii) shows the percentage of NMJ with multiple axonal innervation. No differences were seen between the groups. Thus, there were no specific changes in axonal sprouting, axonal blebs or poly-innervation of NMJ in the i-mnSod1KO group which could not be attributed to the age of the mice.

Images of NMJ show different levels of complexity with significant variability from the “pretzel shape” classically

reported. A scoring system was developed to attempt to quantify and understand whether Sod1KO affected the complexity of the NMJ structure. These ranged from “complex” NMJ with numerous convolutions compared with those which were simply disks with little evidence of internal structure (“basic”). An intermediary level of complexity (“good”) was also used. Examples of “complex,” “good,” and “basic” NMJ are shown in Figure 5d(i),e(i),f(i), and the values obtained from each group are shown in Figure 5d(ii)–f(ii). Approximately 60% of NMJs in adult WT mice had complex junctions with <2% categorized as “basic.” Old i-mnSod1KO mice had the most striking changes with ~40% of NMJs considered to be “basic,” this was a significant increase compared with adult WT ($p < 0.0001$), old WT ($p = 0.0003$), and mid-age i-mnSod1KO ($p < 0.001$). The old i-mnSod1KO ($p < 0.0001$) and Sod1KO ($p = 0.0051$) mice showed a significant decrease in the percentage of “complex” NMJs compared with adult WT. i-mnSod1KO mice therefore showed a significant switch to NMJ having a simple disk structure (i.e., “basic” structure) compared with age-matched WT mice indicating a specific effect of lack of Sod1.

Discussion

Previous studies examining the i-mnSod1KO mouse demonstrated a significant reduction of Sod1 expression in brain, spinal cord and sciatic nerve and concluded that neuron-specific deletion of CuZnSOD is sufficient to cause motor neuron loss in young mice, but loss of innervation may not be sufficient to induce muscle fiber

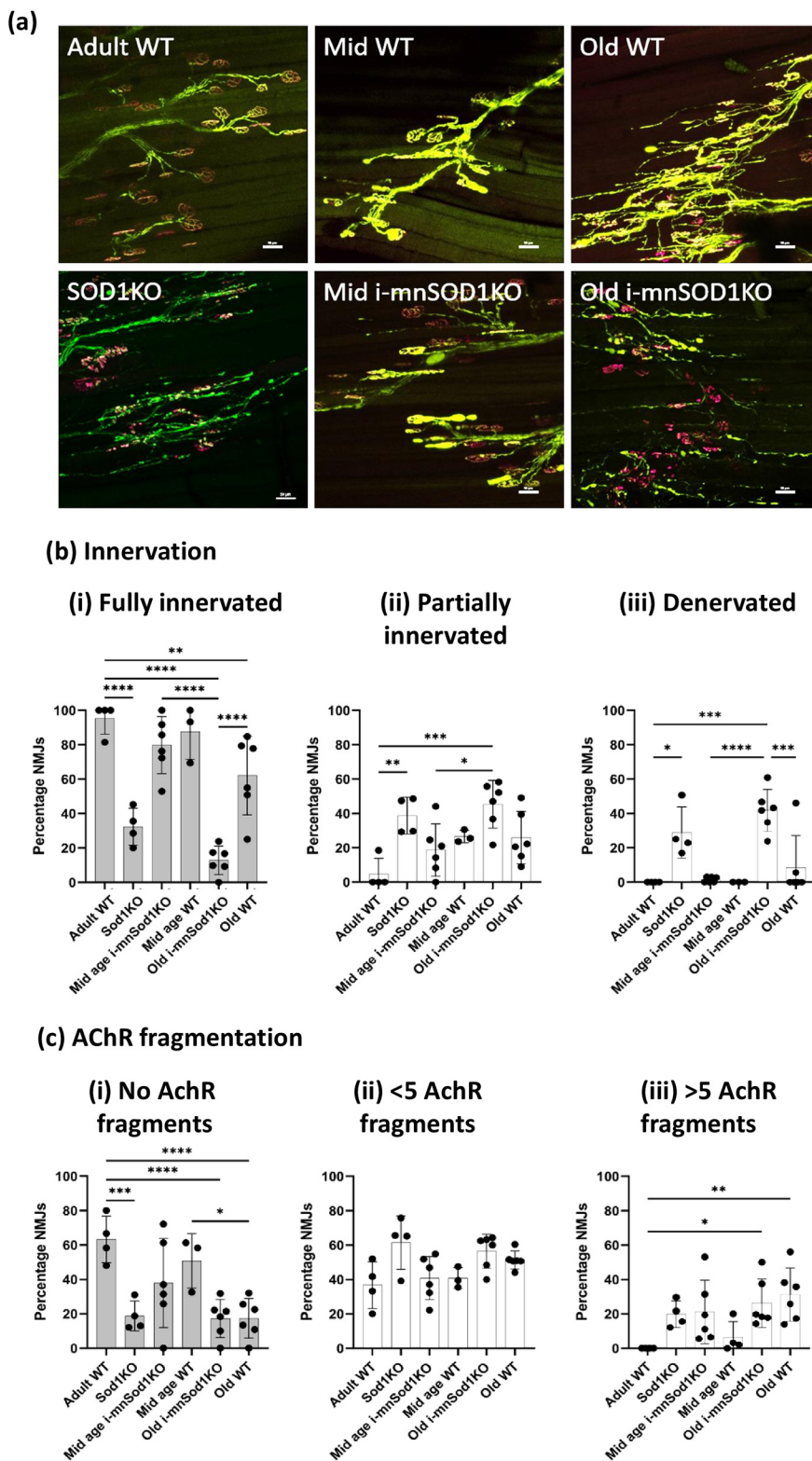


Figure 4. Morphologic assessment of NMJ innervation and fragmentation. Representative images of NMJ and axonal structure seen following bungarotoxin staining (magenta) and Thy1-YFP/CFP (green) visualization in whole EDL muscles from adult, mid-age and old WT, mid-age and old i-mnSod1KO and Sod1KO-Thy1-CFP mice; scale bar = 50 μ m (a). Extent of innervation assessed by percentage overlap of presynaptic nerve terminal and AchR categorized as fully innervated (i), partially innervated (ii) or denervated (iii; b). Average number of AchR fragments reported as none (fully intact; i), <5 (ii), >5 fragments (iii; c). Data are presented as mean \pm SD. Symbols represent significant difference between groups ($*p < 0.05$, $**p < 0.01$, $***p < 0.001$, $****p < 0.0001$) from two-way ANOVA with Tukey's multiple comparison ($n = 4-6$ muscles per group).

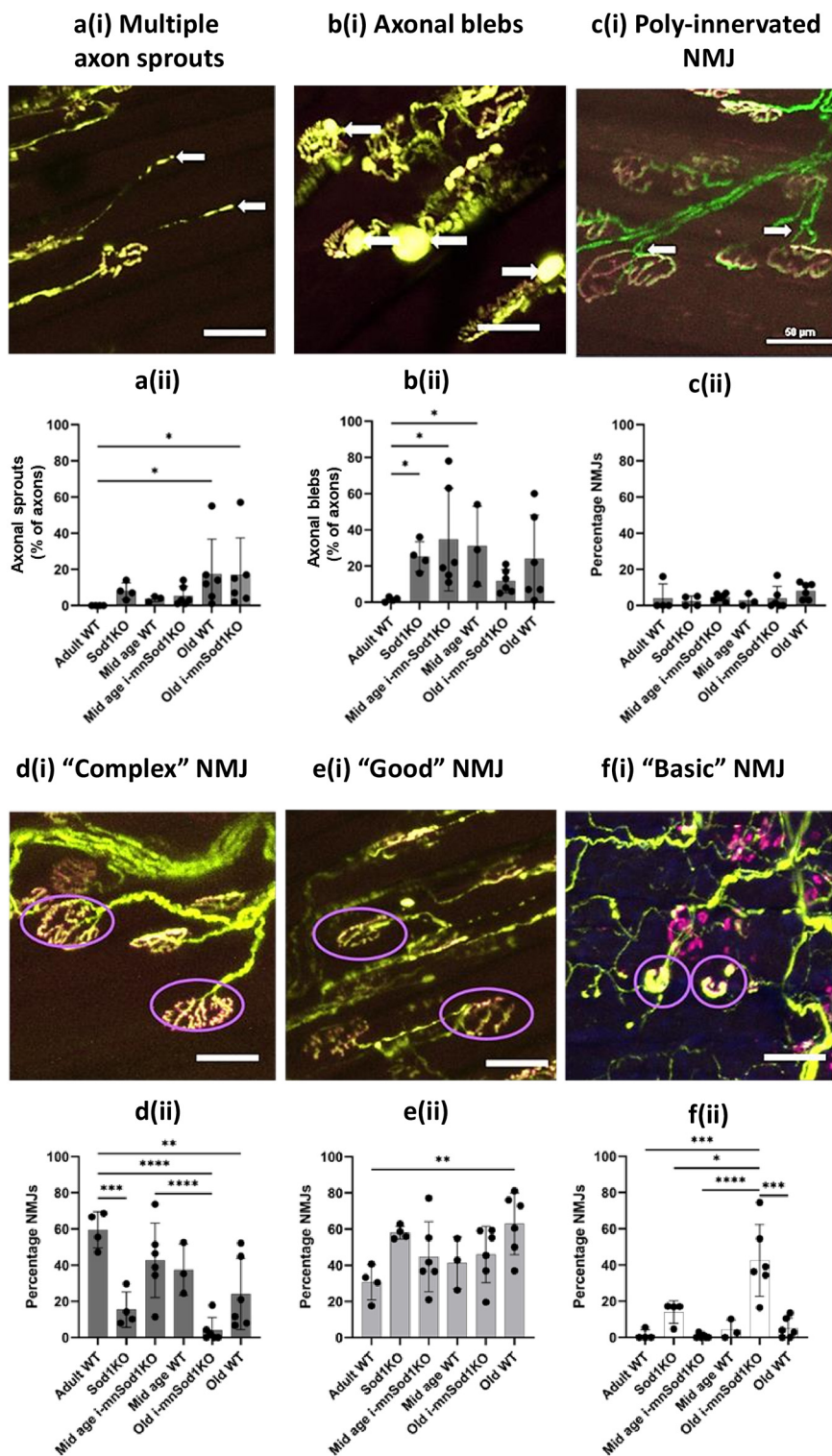


Figure 5. Quantification and representative images of specific NMJ structural alterations in EDL muscle from adult, mid-age and old WT, mid-age and old i-mnSod1KO and Sod1KO-Thy1-CFP mice. As in Figure 4, axons are shown in green and NMJ in magenta. An example of axons with multiple sprouts at **a(i)** with percentage of axons having multiple sprouts, **a(ii)**. Examples of axons with multiple blebs **[b(i)]** with the percentage of axons having blebs **[b(ii)]** and a representative image of poly innervation of NMJ at **c(i)** with the percentage of NMJs which show evidence of multiple innervations at **c(ii)**. Complexity of the NMJ was categorized as complex **[d(i) and d(ii)]**, good **[e(i) and e(ii)]**, or basic **[f(i) and f(ii)]**. Representative images of complex **[d(i)]**, good **[e(i)]**, and basic **[f(i)]** NMJ are shown with the specific NMJ displaying the characteristics circled in purple. Data are presented as mean \pm SD. Symbols represent significant differences between groups based on two-way ANOVA with Tukey's comparison ($n = 4-6$ muscles per group); * $p < 0.05$, ** $p < 0.01$, *** $p < 0.001$, **** $p < 0.0001$.

loss until the muscle reaches a threshold beyond which it cannot compensate for neuronal loss (Bhaskaran et al., 2020). Our aim here was to define the way in which a lack of Sod1 affects neuronal tissue to precipitate the premature age-related loss of muscle mass. Data obtained indicate that by old age, i-mnSod1KO mice showed increased numbers of fully denervated NMJ, a reduced number of large axons and increased number of small axons compared with age-matched WT mice. This was associated with changes in the morphology of the remaining innervated NMJ, which predominantly displayed a less complex structure. In contrast multiple other changes in the nerves and NMJ of old i-mnSod1KO mice (increased protein 3NT content, increased myelin sheath areas, reduced axonal number and fragmentation of NMJs) were also observed in the nerves of old WT mice and appear to be related to aging.

A number of measures of oxidation were examined to determine whether the lack of Sod1 in nerve led to increased oxidation. We previously reported (Sakellariou et al., 2014; McDonagh et al., 2016) that 3-NT and protein carbonyls in nerves did not show a significant increase in old WT mice, Sod1KO mice, nSod1KO or mSod1KO mice, although elevated protein carbonyls in the sciatic nerve of Sod1KO mice has been reported by others (Hamilton et al., 2013). No effect on nerve protein carbonyl contents was seen here, although there was a tendency for nerve protein 3-NT content to increase in both old i-mnSod1KO and old WT mice compared with younger groups. Increased protein 3-NT residues are a mark of oxidation by peroxynitrite which was previously proposed as a mechanism for tissue oxidation in Sod1KO mice (Sakellariou et al., 2011). Tissues were also examined using an EPR technique which previously indicated increased oxidation of the CPH probe in tissues from old compared with adult WT mice (McDonagh et al., 2016). The probe reacts preferentially with superoxide and peroxynitrite and an age-related increase in muscle from WT mice was seen (Extended Data Fig. 1-1). An increase was also seen in the sciatic nerve of Sod1KO mice, but no changes in the nerves of old WT or old i-mnSod1KO mice were detected. Thus, we find no evidence that nerves of i-mnSod1KO mice show an increase in oxidation above that seen in age-matched mice and hence that the premature changes in nerve and NMJ structure and muscle loss are unrelated to increased nerve oxidation. This lack of evidence for major changes in markers of oxidative damage in nerves of i-mnSod1KO mice is compatible with our previous conclusion that the effect of lack of Sod1 in nerves results in impaired redox signaling, rather than oxidative damage, which plays a key role in muscle loss in Sod1KO mice (Sakellariou et al., 2018). Bhaskaran et al. (2020) reported an increased marker of oxidation (F2-isoprostanes) in muscle of old i-mnSod1KO mice compared with old WT mice, but no studies of nerve oxidation were reported.

The previous study of i-mnSod1KO mice (Bhaskaran et al., 2020) examined motor neuron numbers in the ventral spinal cord of mice and reported an estimated early loss of motor neurons in i-mnSod1KO mice which also

occurred with age in WT mice. We have used a retrograde labeling approach which is specific to individual nerves to examine motor neuron numbers. The total number of retrograde labeled sciatic nerve-associated motor neurons in adult mice is remarkably similar to that reported previously (Žygelytė et al., 2016), suggesting that it is a robust method for determining changes in motor neuron numbers. The data showed a substantial (~30%) decline in motor neurons with age for both retrograde gastrocnemius/soleus specific and whole sciatic nerve evaluations which was not exacerbated in the i-mnSod1KO mice (Fig. 3). While this technique does not differentiate between motor neuron subpopulations, α motor neurons make up the largest percentage of efferent neurons innervating a lower limb muscle (Burke et al., 1977; Mierzejewska-Krzyżowska et al., 2019).

Evidence that the lack of Sod1 affected axonal integrity was seen in a loss of axonal area in individual axons of the sciatic nerve of old i-mnSod1KO mice compared with old WT mice. These changes appeared because of a reduction in the proportion of larger axons and a greater proportion of small axons in i-mnSod1KO mice in comparison with adult and old WT (Fig. 2). Together with the lack of decline in total axonal number reported above (Fig. 3), these data appear to indicate an effect of Sod1 in reducing the area of larger axons (and hence increasing the number of smaller axons).

The sciatic nerve also showed an increase in myelin thickness with advanced age as previously reported in other nerves (Peters, 2002). Both old i-mnSod1KO and age matched WT showed increased sheath thickness compared with adult mice. The G-ratio (ratio of the inner axonal diameter to the total outer diameter) is a functional and structural index of optimal axonal myelination (Rushton, 1951; Chomiak and Hu, 2009), but no significant changes were seen between the groups studied. A decreased G-ratio with advancing age has been described in rats (Azcoitia et al., 2003; Amer et al., 2014).

We evaluated in detail the innervation of NMJ, fragmentation of AchRs, numbers of axonal sprouts and blebs, poly-innervation of NMJ, and complexity of the NMJ structure (Figs. 4 and 5). Aging caused loss of innervation, increased fragmentation, increased axonal sprouting and led to a reduced number of complex NMJs (which showed a much simpler structure). A lack of neuronal Sod1 greatly exacerbated the loss of NMJ innervation in older mice and caused an increased proportion of the NMJ to show a simpler structure, but NMJ fragmentation and axonal sprouting were unaffected by lack of Sod1. Both old WT and old i-mnSod1KO mice showed comparable changes in NMJ fragmentation, but comparison with muscle force production indicates that fragmentation may have a limited influence on signaling for force production. Furthermore, it also suggests that a lack of Sod1 in motor neurons has little influence on the postsynaptic complexes that help to maintain NMJ structure.

The lack of neuronal Sod1 in old i-mnSod1KO mice led to accelerated changes in the complexity (pretzel shape) of NMJs with age. Thus, a significant percentage of NMJs in old i-mnSod1KO mice showed similar structure to embryonic (simple fragments) rather than mature pretzel

shaped NMJs. It has been shown (Kang and Lichtman, 2013) that AchR clusters are lost if not re-innervated and the increased presence of NMJs with a pseudo-embryonic structure may reflect a lack of re-innervation in i-mnSod1KO mice which also showed a significant decline in NMJ innervation, in comparison with adult and old WT mice.

Thus, our data indicate that a lack of Sod1 in neuronal tissue leads to an accelerated age-related loss of skeletal muscle mass and function by accelerating or exacerbating a number of the many changes that occur in motor neurons and NMJ with aging. Although previous studies indicated that i-mnSod1KO mice showed loss of motor neurons in the ventral spinal cord compared with that of WT mice (Bhaskaran et al., 2020), we found no additional loss of motor neurons in excess of that which occurs in old WT mice. The assessments of motor neuron numbers in this study and that of Bhaskaran et al. (2020) used different approaches, both of which are likely to have limitations that may have contributed to this divergence. For example, direct counting of motor neurons in sections of the ventral spinal cord may be limited in the ability to detect small motor neurons, while the retrograde labeling approach requires all axonal termini to be accessible to the label and the axons capable of retrograde transport. Lack of neuronal Sod1 led to a greater number of small axons and a reduced number of large axons in the sciatic nerve of old i-mnSod1KO mice in comparison with old WT. Such changes were associated with a substantial reduction in the number of fully innervated NMJ and an increase in the number of denervated NMJ in the i-mnSod1KO mice, while remaining AchR also showed a reversion to an embryonic-type structure. Thus, the data obtained indicate that lack of Sod1 specifically in motor nerves may cause premature muscle atrophy through inducing changes in axonal area, reduction in the relative size of axons, greater overall denervation and modification of NMJ to a less complex structure. It is interesting to speculate why deletion of Sod1 in motor nerves has a greater effect on synaptic structure and integrity in comparison with the effects on the motor neuron cell body. Sod1 plays a well-established role in control of redox signaling and prevention of oxidative damage. The predominance of effects of the deletion in the motor neuron periphery suggests that components of the motor neuron periphery have a greater requirement for controlled redox signaling, or that local prevention of oxidative damage is particularly critical. Whether this relates to differences in the relative dependence on mitochondrial respiration or the overall capacity to prevent oxidative damage is currently unknown.

The question remains as to why the changes in nerve structure and function induced by lack of Sod1 only present as a sarcopenic phenotype in older mice, although the inducible loss of Sod1 in neuronal tissue was reported from 10 months of age. The likely explanation is that appearance of any muscle phenotype is delayed because of expansion of the size of motor units with collateral re-innervation of denervated NMJ. The time delay therefore reflects the period until the ability to expand motor unit size is exceeded. While motor units have a capacity for

expansion to compensate for motor neuron loss, this process may modify and compromise aspects of synaptic transmission (Mantilla and Sieck, 2009; Thomas et al., 2014) and there appears to be a maximum ability to increase the size of an individual motor unit (Thompson and Jansen, 1977). A 25–50% reduction in the number of motor neurons is reported to occur in both man and rodents with aging (Tomlinson and Irving, 1977; Rowan et al., 2012). In humans, Piasecki and colleagues showed that motor unit loss occurred early in the aging process and that failure to expand was characteristic of sarcopenia (Piasecki et al., 2018). Our results are consistent with motor unit loss contributing to decreased force generation with age that is exacerbated by lack of neuronal Sod1 although in both situations the initial loss of neuromuscular integrity is likely to have been mitigated by an ability to expand the size of motor units.

References

- Amer MG, Mazen NF, Mohamed NM (2014) Role of calorie restriction in alleviation of age-related morphological and biochemical changes in sciatic nerve. *Tissue Cell* 46:497–504.
- Azcoitia I, Leonelli E, Magnaghi V, Veiga S, Garcia-Segura LM, Melcangi RC (2003) Progesterone and its derivatives dihydroprogesterone and tetrahydroprogesterone reduce myelin fiber morphological abnormalities and myelin fiber loss in the sciatic nerve of aged rats. *Neurobiol Aging* 24:853–860.
- Bhaskaran S, Pollock N, CM P, Ahn B, Piekarz KM, Staunton CA, Brown JL, Qaisar R, Vasilaki A, Richardson A, McArdle A, Jackson MJ, Brooks SV, Van Remmen H (2020) Neuron-specific deletion of CuZnSOD leads to an advanced sarcopenic phenotype in older mice. *Aging Cell* 19:e13225.
- Brooks SV, Faulkner JA (1988) Contractile properties of skeletal muscles from young, adult and aged mice. *J Physiol* 404:71–82.
- Burke RE, Strick PL, Kanda K, Kim CC, Walmsley B (1977) Anatomy of medial gastrocnemius and soleus motor nuclei in cat spinal cord. *J Neurophysiol* 40:667–680.
- Campbell MJ, McComas AJ, Petito F (1973) Physiological changes in ageing muscles. *J Neurol Neurosurg Psychiatry* 36:174–182.
- Chomiak T, Hu B (2009) What is the optimal value of the g-ratio for myelinated fibers in the rat CNS? A theoretical approach. *PLoS One* 4:e7754.
- Ertürk A, Becker K, Jähring N, Mauch CP, Hojer CD, Egen JG, Hellal F, Bradke F, Sheng M, Dodt HU (2012) Three-dimensional imaging of solvent-cleared organs using 3DISCO. *Nat Protoc* 7:1983–1995.
- Hamilton RT, Bhattacharya A, Walsh ME, Shi Y, Wei R, Zhang Y, Rodriguez KA, Buffenstein R, Chaudhuri AR, Van Remmen H (2013) Elevated protein carbonylation, and misfolding in sciatic nerve from db/db and Sod1(-/-) mice: plausible link between oxidative stress and demyelination. *PLoS One* 8:e65725.
- Jang YC, Lustgarten MS, Liu Y, Muller FL, Bhattacharya A, Liang H, Salmon AB, Brooks SV, Larkin L, Hayworth CR, Richardson A, Van Remmen H (2010) Increased superoxide in vivo accelerates age-associated muscle atrophy through mitochondrial dysfunction and neuromuscular junction degeneration. *FASEB J* 24:1376–1390.
- Kang H, Lichtman JW (2013) Motor axon regeneration and muscle reinnervation in young adult and aged animals. *J Neurosci* 33:19480–19491.
- Larkin LM, Davis CS, Sims-Robinson C, Kostrominova TY, Van Remmen H, Richardson A, Feldman EL, Brooks SV (2011) Skeletal muscle weakness due to deficiency of CuZn-superoxide dismutase is associated with loss of functional innervation. *Am J Physiol Regul Integr Comp Physiol* 301:R1400–R1407.
- Lexell J, Downham D, Sjöström M (1986) Distribution of different fibre types in human skeletal muscles. Fibre type arrangement in

- m. vastus lateralis from three groups of healthy men between 15 and 83 years. *J Neurol Sci* 72:211–222.
- Lexell J, Taylor CC, Sjöström M (1988) What is the cause of the ageing atrophy? Total number, size and proportion of different fiber types studied in whole vastus lateralis muscle from 15- to 83-year-old men. *J Neurol Sci* 84:275–294.
- Mantilla CB, Sieck GC (2009) Neuromuscular adaptations to respiratory muscle inactivity. *Respir Physiol Neurobiol* 169:133–140.
- McDonagh B, Scullion SM, Vasilaki A, Pollock N, McArdle A, Jackson MJ (2016) Ageing-induced changes in the redox status of peripheral motor nerves imply an effect on redox signalling rather than oxidative damage. *Free Radic Biol Med* 94:27–35.
- Mierzejewska-Krzyżowska B, Celichowski J, Bukowska D (2019) The differences in the structure of the motor nucleus of the medial gastrocnemius muscle in male and female rats. *Ann Anat* 221:93–100.
- Narici MV, Maffulli N (2010) Sarcopenia: characteristics, mechanisms and functional significance. *Br Med Bull* 95:139–159.
- Peters A (2002) The effects of normal aging on myelin and nerve fibers: a review. *J Neurocytol* 31:581–593.
- Piasecki M, Ireland A, Piasecki J, Stashuk DW, Swiecicka A, Rutter MK, Jones DA, McPhee JS (2018) Failure to expand the motor unit size to compensate for declining motor unit numbers distinguishes sarcopenic from non-sarcopenic older men. *J Physiol* 596:1627–1637.
- Piekarz KM, Bhaskaran S, Sataranatarajan K, Street K, Premkumar P, Saunders D, Zalles M, Gulej R, Khademi S, Laurin J, Peelor R, Miller BF, Towner R, Van Remmen H (2020) Molecular changes associated with spinal cord aging. *Geroscience* 42:765–784.
- Porter MM, Vandervoort AA, Lexell J (1995) Aging of human muscle: structure, function and adaptability. *Scand J Med Sci Sports* 5:129–142.
- Rowan SL, Rygiel K, Purves-Smith FM, Solbak NM, Turnbull DM, Hepple RT (2012) Denervation causes fiber atrophy and myosin heavy chain co-expression in senescent skeletal muscle. *PLoS One* 7:e29082.
- Rushton WA (1951) A theory of the effects of fibre size in medullated nerve. *J Physiol* 115:101–122.
- Sakellariou GK, Pye D, Vasilaki A, Zibrik L, Palomero J, Kabayo T, McArdle F, Van Remmen H, Richardson A, Tidball JG, McArdle A, Jackson MJ (2011) Role of superoxide-nitric oxide interactions in the accelerated age-related loss of muscle mass in mice lacking Cu,Zn superoxide dismutase. *Aging Cell* 10:749–760.
- Sakellariou GK, Davis CS, Shi Y, Ivannikov MV, Zhang Y, Vasilaki A, Macleod GT, Richardson A, Van Remmen H, Jackson MJ, McArdle A, Brooks SV (2014) Neuron-specific expression of CuZnSOD prevents the loss of muscle mass and function that occurs in homozygous CuZnSOD-knockout mice. *FASEB J* 28:1666–1681.
- Sakellariou GK, McDonagh B, Porter H, Giakoumaki II, Earl KE, Nye GA, Vasilaki A, Brooks SV, Richardson A, Van Remmen H, McArdle A, Jackson MJ (2018) Comparison of whole body SOD1 knockout with muscle-specific SOD1 knockout mice reveals a role for nerve redox signaling in regulation of degenerative pathways in skeletal muscle. *Antioxid Redox Signal* 28:275–295.
- Sataranatarajan K, Qaisar R, Davis C, Sakellariou GK, Vasilaki A, Zhang Y, Liu Y, Bhaskaran S, McArdle A, Jackson M, Brooks SV, Richardson A, Van Remmen H (2015) Neuron specific reduction in CuZnSOD is not sufficient to initiate a full sarcopenia phenotype. *Redox Biol* 5:140–148.
- Sheth KA, Iyer CC, Wier CG, Crum AE, Bratasz A, Kolb SJ, Clark BC, Burghes AHM, Arnold WD (2018) Muscle strength and size are associated with motor unit connectivity in aged mice. *Neurobiol Aging* 67:128–136.
- Sonjak V, Jacob K, Morais JA, Rivera-Zengotita M, Spendiff S, Spake C, Taivassalo T, Chevalier S, Hepple RT (2019) Fidelity of muscle fibre reinnervation modulates ageing muscle impact in elderly women. *J Physiol* 597:5009–5023.
- Staunton CA, Owen ED, Pollock N, Vasilaki A, Barrett-Jolley R, McArdle A, Jackson MJ (2019) HyPer2 imaging reveals temporal and heterogeneous hydrogen peroxide changes in denervated and aged skeletal muscle fibers in vivo. *Sci Rep* 9:14461.
- Thomas CK, Bakels R, Klein CS, Zijdwind I (2014) Human spinal cord injury: motor unit properties and behaviour. *Acta Physiol* 210:5–19.
- Thompson W, Jansen JK (1977) The extent of sprouting of remaining motor units in partly denervated immature and adult rat soleus muscle. *Neuroscience* 2:523–535.
- Tomlinson BE, Irving D (1977) The numbers of limb motor neurons in the human lumbosacral cord throughout life. *J Neurol Sci* 34:213–219.
- Vasilaki A, Pollock N, Giakoumaki I, Goljanek-Whysall K, Sakellariou GK, Pearson T, Kayani A, Jackson MJ, McArdle A (2016) The effect of lengthening contractions on neuromuscular junction structure in adult and old mice. *Age (Dordr)* 8:259–272.
- Žygelytė E, Bernard ME, Tomlinson JE, Martin MJ, Terhorst A, Bradford HE, Lundquist SA, Sledziona M, Cheatham J (2016) RetroDISCO: clearing technique to improve quantification of retrograde labeled motor neurons of intact mouse spinal cords. *J Neurosci Methods* 271:34–42.